ANL-77-88

# APPROXIMATIONS OF GAMMA CROSS SECTIONS FOR FAST NUCLEAR REACTORS

by

K. N. Grimm and D. Meneghetti

BASE TECHNOLOGY

U of C-AUA-USDOE

ARGONNE NATIONAL LABORATORY, ARGONNE, ILLINOIS

Prepared for the U. S. DEPARTMENT OF ENERGY
under Contract W-31-109-Eng-38

Printed in the United States of America
Available from
National Technical Information Service
U. S. Department of Commerce
5285 Port Royal Road
Springfield, Virginia 22161
Price: Printed Copy $4.00; Microfiche $3.00

Distribution Category:
LMFBR Physics (UC-79d)

ANL-77-88

ARGONNE NATIONAL LABORATORY
9700 South Cass Avenue
Argonne, Illinois 60439

# APPROXIMATIONS OF GAMMA CROSS SECTIONS FOR FAST NUCLEAR REACTORS

by

K. N. Grimm and D. Meneghetti

EBR-II Project

March 1978

# TABLE OF CONTENTS

# LIST OF FIGURES

# LIST OF TABLES

# APPROXIMATIONS OF GAMMA CROSS SECTIONS FOR FAST NUCLEAR REACTORS

by

K. N. Grimm and D. Meneghetti

## ABSTRACT

This report shows a method to approximate a $P_1$ scattering solution for the flux in a fast reactor, using an isotropic, but not a diagonal-transport-approximation scattering matrix. Presented are flux errors relative to a $P_1$ solution for different levels of transport approximation in an EBR-II type of core surrounded by a stainless steel reflector. Problems associated with the use of the method are also presented.

## I. INTRODUCTION

For calculation of the neutron environment in Experimental Breeder Reactor II (EBR-II), the diagonal-transport approximation ($P_0^T$) with $S_4$ angular quadrature gives satisfactory results.[1] For calculation of the gamma environment, however, scattering cross sections of a higher order must be used.[1] Use of those cross sections increases calculation time, requirements for computer storage of cross sections, and dependence on anisotropic-transport codes. Therefore, we investigated the possibility of making gamma calculations with an "extended" diagonal-transport approximation that takes into account the effects of higher-order scattering cross sections other than those on the diagonal. This approximation is called the "full-transport" approximation here and is symbolized by $P_0^F$. Determined were the spatial variations of cross sections for full-transport approximation that would simulate a solution based on $P_1$ scattering, but would retain an isotropic scattering matrix. Also investigated were solutions generated using a current- and area-weighted average of these spatially dependent cross sections.

## II. THEORY

The cross sections for the full-transport approximation are derived from the one-dimensional Boltzmann equation for steady state, with the scattering cross section and flux (in the scattering integral) expanded in Legendre polynominals:

$$\mu \frac{\partial \varphi_g(x,\mu)}{\partial x} + \Sigma_t^g(x)\varphi_g(x,\mu) = \sum_{g'} \sum_{\ell=0}^{\infty} \frac{2\ell+1}{2} \Sigma_{s\ell}^{g' \to g}(x) P_\ell(\mu) \varphi_{g',\ell}(x),$$

where

$\varphi_g(x,\mu)$ = angular flux at position x and angle $\mu$ for energy group g,

$\varphi^{\ell}_{g'}(x)$ = $\ell$th moment of the angular flux at position x for energy group g',

$\Sigma^g_t(x)$ = macroscopic total cross section at position x for energy group g,

$\Sigma^{g'\to g}_{s\ell}(x)$ = $\ell$th moment of the macroscopic scattering cross section at position x for scattering from energy group g' to energy group g,

and

$P_\ell(\mu)$ = $\ell$th Legendre polynominal.

Substituting into the above equation the Legendre expansion for the flux, multiplying by the Legendre polynominal $P_n(\mu)$, and integrating from -1 to +1 give

$$\sum_{\ell=0}^{\infty}\left[\frac{2\ell+1}{2}\frac{\partial\varphi^{\ell}_g(x)}{\partial x}\int_{-1}^{1}P_1(\mu)P_\ell(\mu)P_n(\mu)d\mu + \Sigma^g_t(x)\varphi^{\ell}_g(x)\delta_{\ell,n} - \sum_{g'}\Sigma^{g'\to g}_{s\ell}(x)\varphi^{\ell}_{g'}(x)\delta_{\ell,n}\right] = 0,$$

where

$$\delta_{\ell,n} = \text{Kronecker delta function} = \begin{cases}1, & \ell = n\\ 0, & \ell \neq n.\end{cases}$$

The equations for n = 0 and n = 1, with the summation on $\ell$ going from zero to one, are the consistent $P_1$ equations. They are

$$\frac{\partial\varphi^1_g(x)}{\partial x} + \left[\Sigma^g_t(x) - \Sigma^{g\to g}_{s0}(x)\right]\varphi^0_g(x) - \sum_{g'\neq g}\Sigma^{g'\to g}_{s0}(x)\varphi^0_{g'}(x) = 0$$

and

$$\frac{1}{3}\frac{\partial\varphi^0_g(x)}{\partial x} + \left[\Sigma^g_t(x) - \Sigma^{g\to g}_{s0}(x)\right]\varphi^1_g(x) - \sum_{g'\neq g}\Sigma^{g'\to g}_{s1}(x)\varphi^1_{g'}(x) = 0.$$

These equations can be made equivalent to the corresponding equations for isotropic scattering if the following redefinitions for the total and the scattering cross sections are made:

$$\left[\Sigma_t^g(x)\right]^{\text{Full}} = \Sigma_t^g(x) - \Sigma_{s1}^{g\to g}(x) - \sum_{g'\neq g} \Sigma_{s1}^{g'\to g}(x)\frac{\varphi_{g'}^1(x)}{\varphi_g^1(x)},$$

$$\left[\Sigma_{s0}^{g\to g}(x)\right]^{\text{Full}} = \Sigma_{s0}^{g\to g}(x) - \Sigma_{s1}^{g\to g} - \sum_{g'\neq g} \Sigma_{s1}^{g'\to g}(x)\frac{\varphi_{g'}^1(x)}{\varphi_g^1(x)},$$

and

$$\left[\Sigma_{s0}^{g'\to g}(x)\right]^{\text{Full}} = \Sigma_{s0}^{g'\to g}(x).$$

The above equations define the full-transport approximation.

The cross section for the diagonal-transport approximation is obtained by ignoring the first moment of the downscatter cross sections; hence,

$$\left.\begin{aligned}\left[\Sigma_t^g(x)\right]^{\text{Diagonal}} &= \Sigma_t^g(x) - \Sigma_{s1}^{g\to g}(x) = \Sigma_t^g(x) - \bar{\mu}_{g\to g}\Sigma_{s0}^{g\to g}\\ \text{and}\\ \left[\Sigma_{s0}^{g\to g}(x)\right]^{\text{Diagonal}} &= \Sigma_{s0}^{g\to g}(x) - \Sigma_{s1}^{g\to g}(x) = \Sigma_{s0}^{g\to g}(x) - \bar{\mu}_{g\to g}\Sigma_{s0}^{g\to g}(x),\end{aligned}\right\} \quad (1)$$

where $\bar{\mu}_{g\to g}$ is the average angle of scatter for ingroup scattering. The full-transport cross sections can be written in the same format as the diagonal-transport cross sections, but $\bar{\mu}_{g\to g}$ is replaced by a space-dependent weighted mean angle of scatter ($\langle\mu(x)\rangle$):

$$\left.\begin{aligned}\left[\Sigma_t^g(x)\right]^{\text{Full}} &= \Sigma_t^g(x) - \langle\mu(x)\rangle\Sigma_{s0}^{g\to g}\\ \text{and}\\ \left[\Sigma_{s0}^{g\to g}(x)\right]^{\text{Full}} &= \Sigma_{s0}^{g\to g} - \langle\mu(x)\rangle\Sigma_{s0}^{g\to g}\end{aligned}\right\} \quad (2)$$

(Contd.)

where (Contd.)

$$\left.\begin{aligned}\langle\mu(x)\rangle &= \sum_{g'} \bar{\mu}_{g'\to g}\left(\frac{\Sigma_{s0}^{g'\to g}(x)}{\Sigma_{s0}^{g\to g}(x)}\right)\frac{\varphi_{g'}^{1}(x)}{\varphi_{g}^{1}(x)} \\ &= \bar{\mu}_{g\to g} + \sum_{g'\neq g} \bar{\mu}_{g'\to g}\left(\frac{\Sigma_{s0}^{g'\to g}(x)}{\Sigma_{s0}^{g\to g}(x)}\right)\frac{\varphi_{g'}^{1}(x)}{\varphi_{g}^{1}(x)}\end{aligned}\right\} \quad (2)$$

and $\bar{\mu}_{g'\to g}$ is the average angle of scatter for scattering from group g' to group g.

There are three difficulties to the use of full-transport cross sections: (1) A current is needed, so we have to have some estimate of the current before we can do the problem; (2) the current is spatially dependent in a homogeneous region, so the full-transport cross sections will be heterogeneous in a homogeneous region; (3) problems arise when the spatial ingroup current is zero.

To circumvent the limitations imposed by space dependency of the cross sections, the average cross sections for the full-transport approximation ($\langle P_0^F \rangle$) were also investigated. The region-dependent average transport cross section for the full-transport approximation is defined as

$$\langle\Sigma_t^g\rangle^{\text{Full}} = \frac{\int_r \left[\Sigma_t^g(r)\right]^{\text{Full}}\varphi_g^1(r)r\,dr}{\int_r \varphi_g^1(r)r\,dr}. \quad (3)$$

The full-transport ingroup scattering cross section also has to be modified to preserve the removal cross section.

## III. MODEL DESCRIPTION AND METHOD OF SOLUTION

The study was made for an idealized, one-dimensional, homogeneous cylindrical fast-reactor core of the EBR-II type surrounded by a homogeneous stainless steel reflector (see Fig. 1). The core-smeared number densities were generated by smearing a two-dimensional (X-Y) description of an actual EBR-II core loading. The core fuel enrichment was 66% (63% $^{235}$U and 3% $^{239}$Pu) The number densities used in the calculation are shown in Table I.

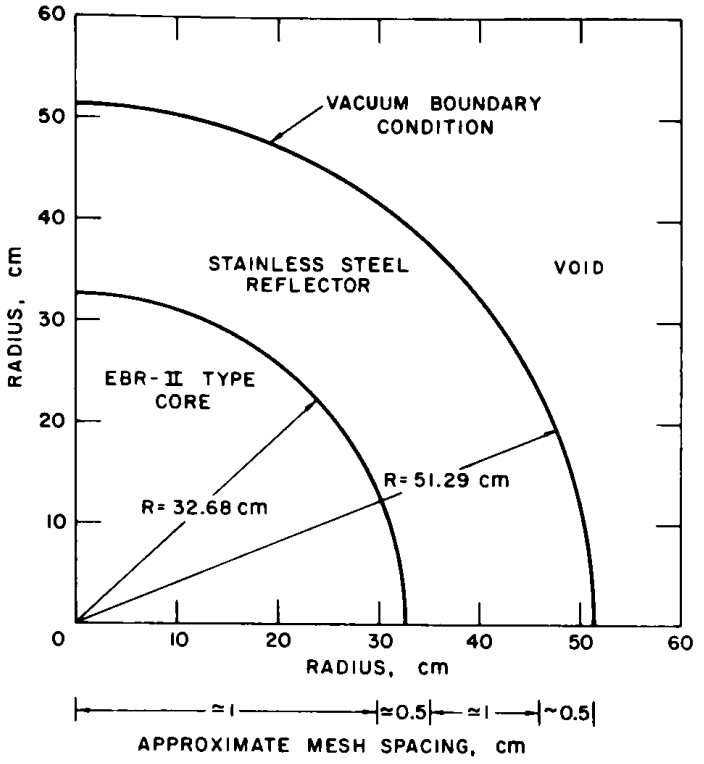


Fig. 1. Model Description

TABLE I. Smeared Densities Used for Model

| Core | | Reflector | |
|---|---|---|---|
| Element | Density[a] | Element | Density[a] |
| $^{235}U$ | $4.72 \times 10^{-3}$ | Fe | $4.71 \times 10^{-2}$ |
| $^{238}U$ | $2.55 \times 10^{-3}$ | Ni | $5.91 \times 10^{-3}$ |
| $^{239}Pu$ | $2.16 \times 10^{-4}$ | Cr | $1.30 \times 10^{-2}$ |
| Fe | $1.84 \times 10^{-2}$ | Na | $4.80 \times 10^{-3}$ |
| Ni | $2.43 \times 10^{-3}$ | | |
| Cr | $4.91 \times 10^{-3}$ | | |
| Na | $1.00 \times 10^{-2}$ | | |
| O | $1.88 \times 10^{-3}$ | | |
| Mo | $4.60 \times 10^{-4}$ | | |
| Nb | $2.40 \times 10^{-6}$ | | |
| Zr | $3.76 \times 10^{-4}$ | | |
| U5FP1[b] | $4.00 \times 10^{-7}$ | | |
| U5FP2[c] | $3.13 \times 10^{-5}$ | | |
| U5FP3[d] | $1.29 \times 10^{-4}$ | | |

[a] In units of $cm^{-1}$/barn; 1 barn = $1 \times 10^{-28}$ $m^2$.
[b] A rapidly saturating $^{235}U$ lumped fission-product chain.
[c] A slowly saturating $^{235}U$ lumped fission-product chain.
[d] A nonsaturating $^{235}U$ lumped fission-product chain.

The transport calculations were done using the one-dimensional transport code ANISN.[2] There were 34 mesh points in the core and 26 in the reflector. The mesh spacing was about 1 cm, except near boundaries, where it was about 0.5 cm. The gamma-source distribution was generated using gamma-production cross sections generated from the POPOP4 library[3] and with the POPOP4 code.[4] The neutron-flux eigenvalue was calculated with $S_4$ angular quadrature and a 29-group diagonal-transport isotropic neutron-transport cross-section set generated by the $MC^2$ code[5] from ENDF/B cross sections. Fixed-source gamma-transport calculations were done using $S_4$ angular quadrature and a 20-energy-group cross-section set generated by the MUG code.[6]

## IV. DIFFICULTIES IN CALCULATING FULL-TRANSPORT CROSS SECTIONS

If the spatial currents needed in the full-transport method are calculated near a reversal in the in-group current ($\varphi_g^1$), the spatially dependent correction term in the full-transport approximation may become large and oscillatory. Two examples of effects of spatially dependent singularity are shown in Table II. In the group-2 example, the ratio of the transport cross section for the full-transport approximation to the isotropic total cross section is between 0.95 and 0.98 for all reflector mesh points except 41, where the ratio is 45.3. Also shown in Table II is a singularity effect in group 19. These effects of spatially dependent singularities were circumvented by using interpolation based on nearest neighbors (or extrapolation near boundaries) in the cross section. In the group-2 example, the interpolated value of 0.962 was used as the true ratio instead of 45.3.

TABLE II. Examples of Singularities in Full-transport Cross Section

| Group 2 (7 → 8 MeV) | | Group 19 (0.1 → 0.2 MeV) | |
|---|---|---|---|
| Mesh Point (Reflector) | $\frac{\Sigma_{Tr}^{Full}}{\Sigma_{Tot}}$ [a] | Mesh Point (Reflector) | $\frac{\Sigma_{Tr}^{Full}}{\Sigma_{Tot}}$ [a] |
| 38 | 0.967 | 36 | 0.704 |
| 39 | 0.967 | 37 | 0.506 |
| 40 | 0.978 | 38 | 0.021 (1.03)[b] |
| 41 | 45.3 (0.962)[b] | 39 | -2.15 (1.57)[b] |
| 42 | 0.951 | 40 | 7.08 (2.10)[b] |
| 43 | 0.956 | 41 | 2.64 |
| 44 | 0.956 | 42 | 2.03 |
| | | 43 | 1.94 |
| | | 44 | 1.93 |
| | | 45 | 1.93 |
| $\left(\frac{\Sigma_{Tr}^{Diagonal}}{\Sigma_{Tot}}\right)_{Refl}^{c}$ | = 0.973 | $\left(\frac{\Sigma_{Tr}^{Diagonal}}{\Sigma_{Tot}}\right)_{Refl}^{c}$ | = 0.846 |

[a] Full transport, using $P_1$ currents.
[b] Interpolated values (see text).
[c] Diagonal transport.

The question arose as to what criteria should be used to judge when and spatially how far interpolation should be performed. As seen in Table II, the group-2 example was fairly straightforward, but in the group-19 example, it was not clear as to how far on either side of the obviously bad value at mesh point 39 interpolated values should be used. In cases such as this, interpolated values were used over wide enough spatial ranges to provide reasonably smooth transitions of the values for transport cross section. In the calculation using the model, nine (out of 1200) transport cross sections for the full-transport approximation were smoothed out because of abrupt discontinuities in cross section.

When there is not a current reversal, full-transport cross sections can be unrealistic if an in-group current is small relative to the out-of-group currents. This effect was noted in the model calculation for energies below 0.2 MeV (groups 19 and 20) in certain regions. Table III gives an example of this effect. The table shows the ratios of full-transport-approximation transport cross section to total cross section for group 20 in a fraction of the reflector region. No interpolation scheme seemed reasonable for any of the points. In fact, some regions had a large number of negative full-transport-approximation transport cross sections. This problem was circumvented by using the diagonal-transport-approximation transport cross section, thereby ignoring the current-related correction term, in the energy groups and regions where this effect was seen. This procedure was used in group 19 in the core and group 20 in the reflector. Using diagonal-transport cross sections in these groups will not lead to significant errors, because diagonal transport is a reasonable assumption for the core (see Fig. 2) and absorption, not scattering, is the dominant effect in group 20 in the reflector.

TABLE III. Example of Effect of Relatively Small In-group Currents on Full-transport Cross Section

| Group 20 (0.01 → 0.1 MeV) | | Group 20 (0.01 → 0.1 MeV) | |
|---|---|---|---|
| Mesh Point (Reflector) | $\frac{\Sigma_{Tr}^{Full}}{\Sigma_{Tot}}$ [a] | Mesh Point (Reflector) | $\frac{\Sigma_{Tr}^{Full}}{\Sigma_{Tot}}$ [a] |
| 35 | -0.073 | 42 | -0.558 |
| 36 | -0.101 | 43 | -0.241 |
| 37 | 0.083 | 44 | -0.307 |
| 38 | -0.163 | 45 | -0.273 |
| 39 | 0.443 | 46 | 0.001 |
| 40 | 0.299 | 47 | -0.328 |
| 41 | -0.400 | 48 | 0.037 |

$$\left(\frac{\Sigma_{Tr}^{Diagonal}}{\Sigma_{Tot}}\right)_{Refl}^{b} = 0.998$$

[a] Full transport, using $P_1$ currents.
[b] Diagonal transport.

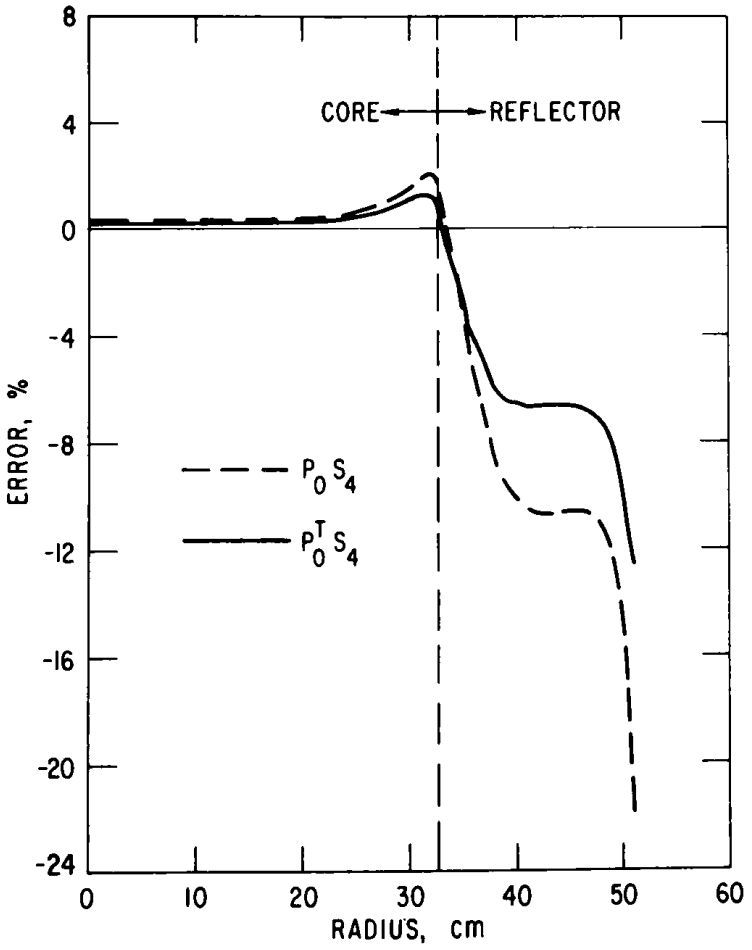


Fig. 2

Relative Error in Total Gamma Flux: $P_0S_4$ and $P_0^TS_4$ vs $P_1S_4$

The smoothed space-dependent full-transport-approximation cross sections were used in all full-transport calculations and were also used when the average full-transport cross sections were calculated.

## V. RESULTS

Since the full-transport approximation can at best only approximate a solution based on $P_1$ scattering, one has to ensure that the $P_1$ solution for the problem under consideration is adequate. Figure 3 shows the error in the total gamma flux from a $P_1S_4$ calculation relative to that from a $P_3S_8$ calculation of the model calculation. The error is defined as

$$\frac{\text{Flux}(P_3S_8) - \text{Flux}(P_1S_4)}{\text{Flux}(P_3S_8)} \times 100.$$

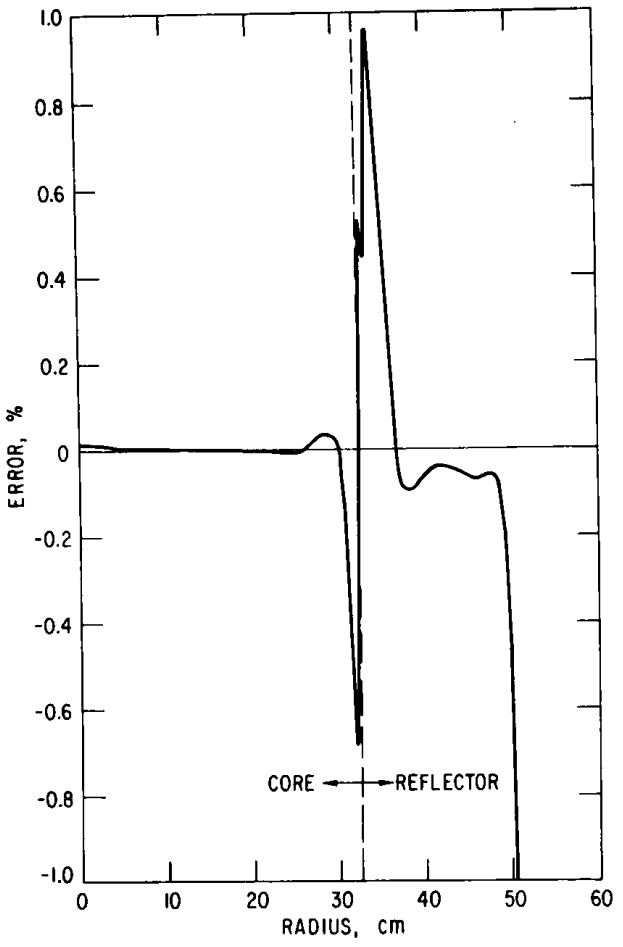


Fig. 3. Relative Error in Total Gamma Flux: $P_1S_4$ vs $P_3S_8$

The maximum relative error in the total flux is about 1%, whereas the maximum relative error in any groupwise flux is less than 2%. Hence, for the problem under consideration, a $P_1$ solution is adequate.

Figure 2 shows the errors relative to a $P_1$ calculation when isotropic ($P_0S_4$) and diagonal-transport ($P_0^TS_4$) cross sections were used. The maximum relative error in the reflector region can be in the range of 10-20%, whereas the maximum relative error in the core is only a few percent. The error in the reflector is larger than that in the core because of the imbalance of isotropic source between the two regions (see Fig. 4). This imbalance leads to a more anisotropic flux distribution in the reflector because of gamma transport from the source-rich core to the source-poor reflector (see Figs. 5 and 6).

Since anisotropic scattering cross sections are important only to the solution for flux where anisotropic fluxes exist,[7] the solution for flux in the reflector is more dependent on the higher-order moments of the scattering cross section than the solution for flux in the core. Thus, when the higher-order moments of the scattering are totally ignored, as for the isotropic cross sections, and almost totally ignored--except for the in-group $P_1$ scattering cross section ($\Sigma_{s1}^{g\rightarrow g}$)--as for the diagonal-transport-approximation cross sections, the relative error in the reflector should be larger.

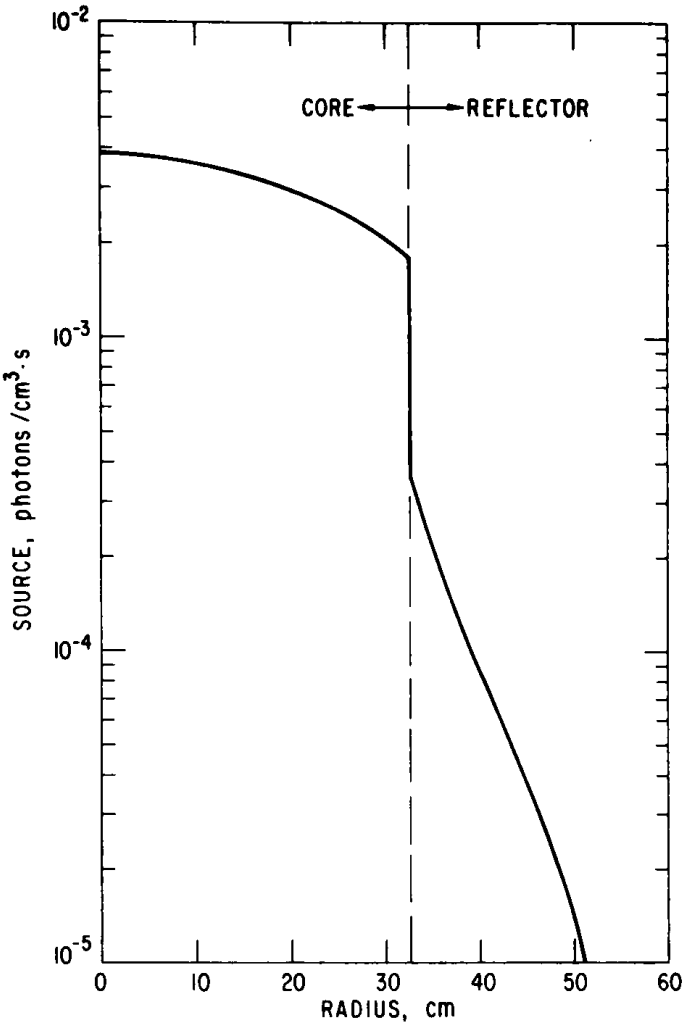


Fig. 4. Radial Distribution of Total Gamma Source in Core and Reflector

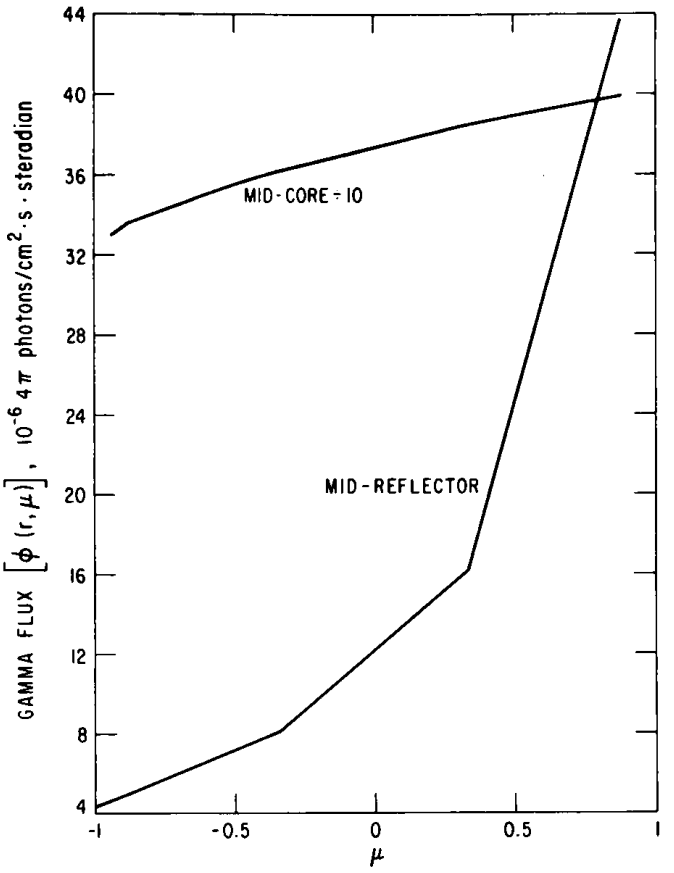


Fig. 5. Angular Gamma Flux for Group 12 at Midcore and Midreflector

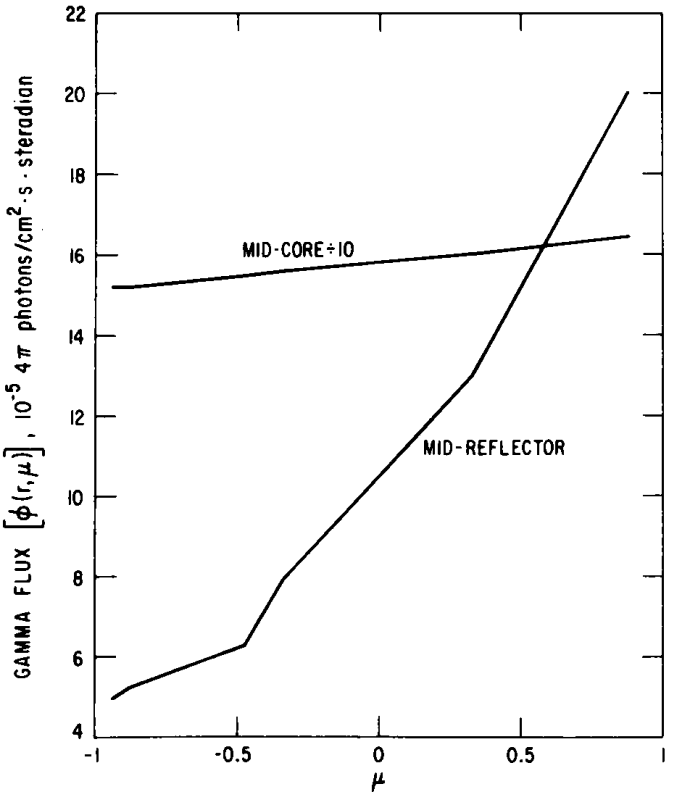


Fig. 6

Angular Gamma Flux for Group 17 at Midcore and Midreflector

As was mentioned in Sec. II, the full-transport cross sections are functions of an estimated current for the calculation. The currents for the model problem, calculated using $P_1$ cross sections and diagonal-transport cross sections, are shown in Figs. 7 and 8 for the representative groups 12 and 17. The values are reasonably similar, and hence currents from a diagonal-transport gamma solution could be used, without introducing much additional error, in determining the full-transport-approximation cross sections.

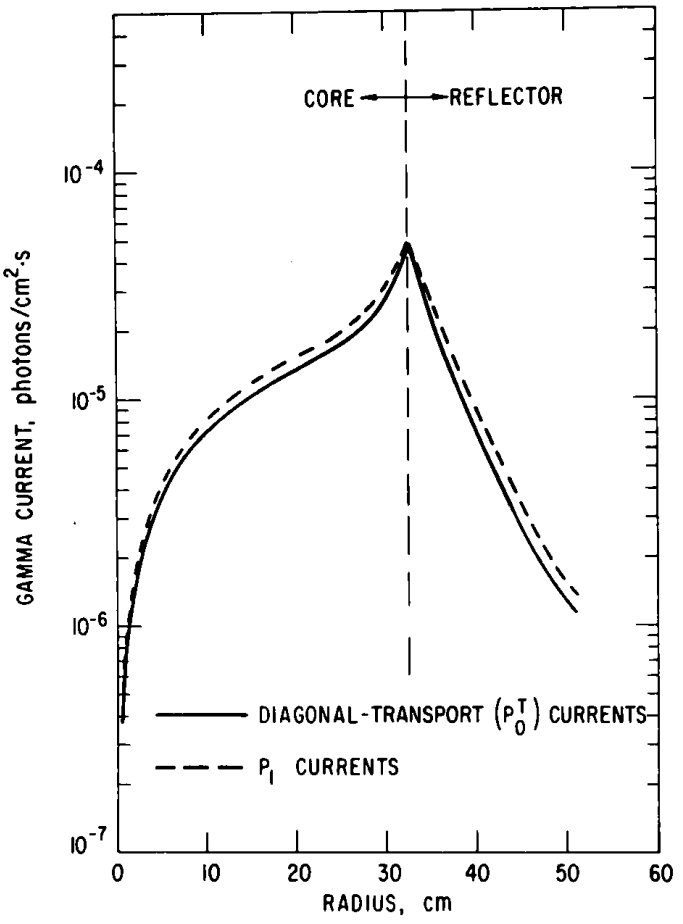


Fig. 7. Radial Distribution of Group-12 Gamma Currents in Core and Reflector

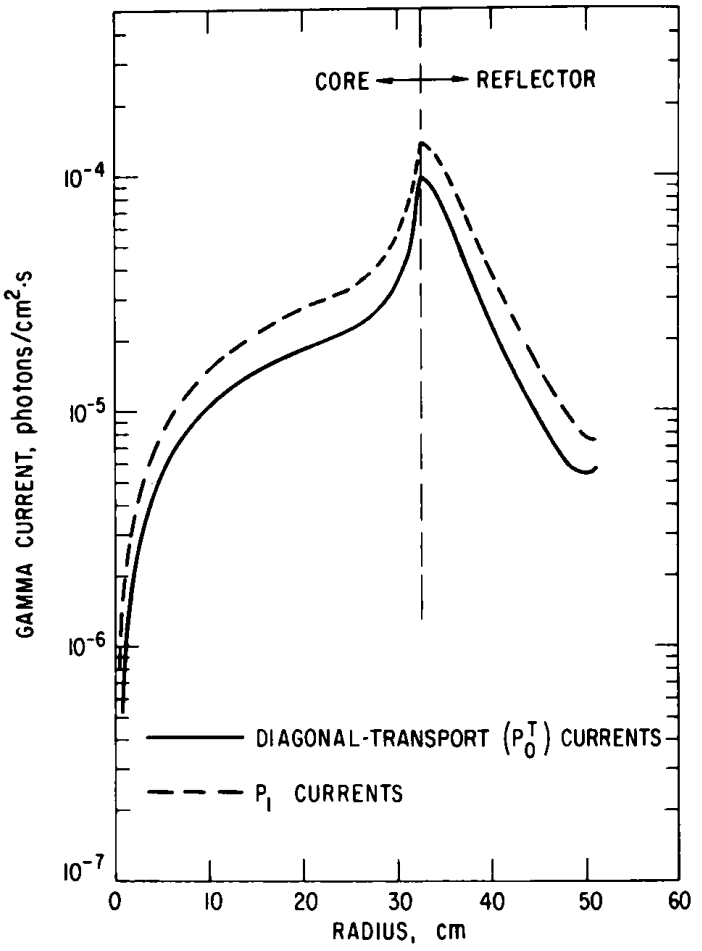


Fig. 8. Radial Distribution of Group-17 Gamma Currents in Core and Reflector

In the model calculation, average full-transport-approximation cross sections were calculated using currents generated from a diagonal-transport solution. Two examples of the differences between isotropic, diagonal-transport, and full-transport-approximation cross sections are shown in Figs. 9 and 10 for energy groups 12 and 17. Plotted are the constant values of total isotropic cross section ($P_0$) and diagonal-transport-approximation transport cross section ($P_0^T$), the spatially dependent full-transport-approximation transport cross section ($P_0^F$), and the full-transport-approximation transport cross section averaged with diagonal-transport currents $\langle P_0^F \rangle$.

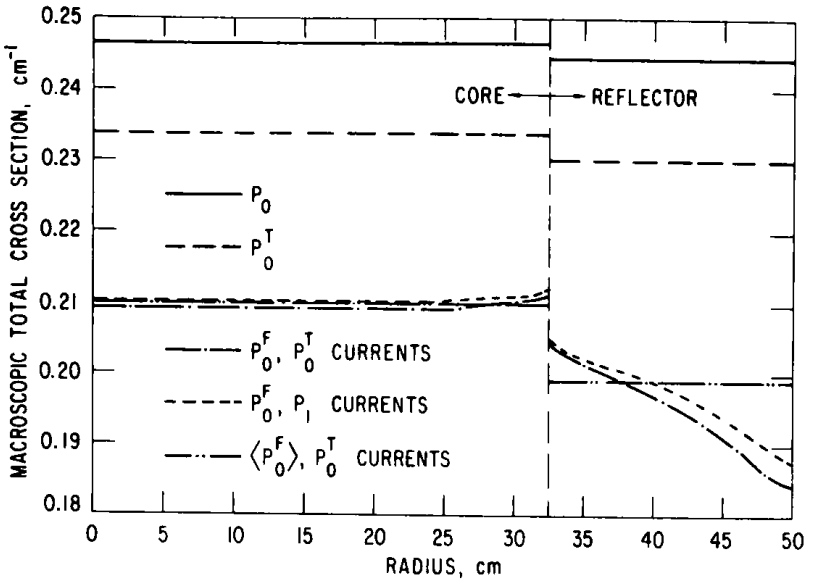


Fig. 9

Group-12 Gamma Macroscopic Total Cross Sections

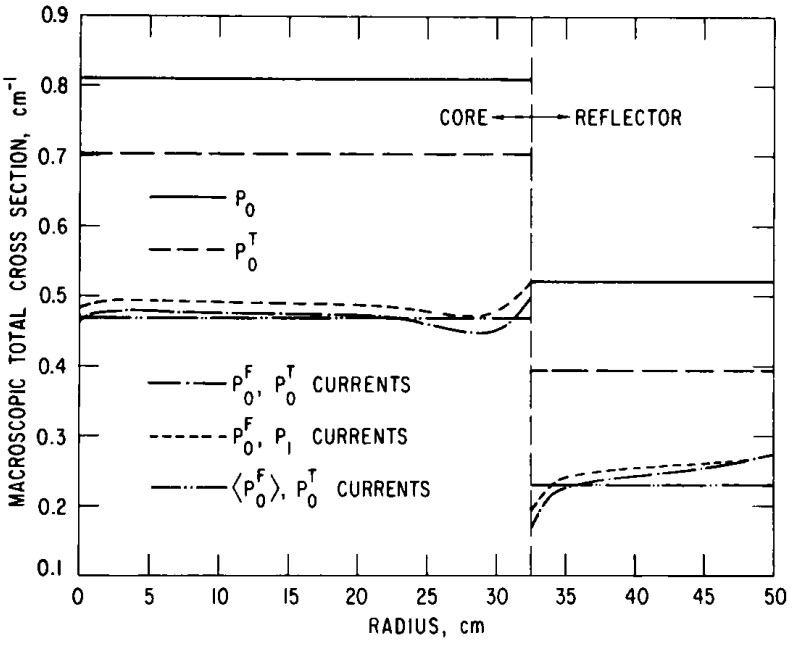


Fig. 10

Group-17 Gamma Macroscopic Total Cross Sections

In the core and reflector regions, the diagonal-transport-approximation transport cross section was smaller than the total cross section, because $\bar{\mu}_{g \to g}$ is positive (see Eq. 1). In those regions, however, the full-transport-approximation transport cross section normally was smaller than either the total or diagonal-transport-approximation transport cross section, because the values for $\bar{\mu}_{g' \to g}$ are positive (see Eq. 2) and, in the model problem, most of the currents were positive. At some mesh points for some energy groups, however, the presence of negative currents caused the full-transport-approximation transport cross sections to be larger than the diagonal-transport-approximation transport and total cross sections.

In addition, near the core-reflector interface in both the core and reflector regions, where the flux is more anisotropic, the full-transport-approximation transport cross sections are strongly spatially dependent. Table IV shows the energy dependence of the isotropic, diagonal-transport, and current-weighted average full-transport-approximation cross sections.

In several groups, the average full-transport-approximation transport cross section was larger than the maximum spatial value. This was due to the fact that in the averaging scheme (see Eq. 3), there were current reversals.

TABLE IV. Energy Dependence of Different Cross Sections

| Group | Upper Energy, MeV | Core | | | Reflector | | |
|---|---|---|---|---|---|---|---|
| | | $P_0$[a] | $P_0^T$[b] | $\langle P_0^F \rangle$, $P_0^T$[c] | $P_0$ | $P_0^T$ | $\langle P_0^F \rangle$, $P_0^T$ |
| 1 | 10.0 | 0.229 | 0.225 | 0.225 | 0.183 | 0.178 | 0.178 |
| 2 | 8.0 | 0.223 | 0.219 | 0.224 | 0.183 | 0.179 | 0.176 |
| 3 | 7.0 | 0.221 | 0.219 | 0.219 | 0.184 | 0.182 | 0.153 |
| 4 | 6.5 | 0.220 | 0.216 | 0.215 | 0.186 | 0.183 | 0.166 |
| 5 | 6.0 | 0.220 | 0.217 | 0.214 | 0.189 | 0.186 | 0.169 |
| 6 | 5.5 | 0.221 | 0.218 | 0.213 | 0.193 | 0.189 | 0.171 |
| 7 | 5.0 | 0.221 | 0.217 | 0.211 | 0.197 | 0.192 | 0.177 |
| 8 | 4.5 | 0.221 | 0.216 | 0.219 | 0.201 | 0.195 | 0.182 |
| 9 | 4.0 | 0.224 | 0.217 | 0.207 | 0.208 | 0.201 | 0.188 |
| 10 | 3.5 | 0.230 | 0.221 | 0.206 | 0.219 | 0.209 | 0.188 |
| 11 | 3.0 | 0.237 | 0.228 | 0.207 | 0.231 | 0.220 | 0.197 |
| 12 | 2.6 | 0.246 | 0.234 | 0.210 | 0.244 | 0.230 | 0.199 |
| 13 | 2.2 | 0.264 | 0.246 | 0.212 | 0.266 | 0.245 | 0.203 |
| 14 | 1.8 | 0.296 | 0.265 | 0.220 | 0.297 | 0.262 | 0.208 |
| 15 | 1.35 | 0.370 | 0.314 | 0.242 | 0.352 | 0.288 | 0.210 |
| 16 | 0.9 | 0.519 | 0.440 | 0.292 | 0.430 | 0.339 | 0.198 |
| 17 | 0.6 | 0.811 | 0.703 | 0.468 | 0.520 | 0.394 | 0.229 |
| 18 | 0.4 | 1.990 | 1.800 | 3.425 | 0.682 | 0.461 | 5.274 |
| 19 | 0.2 | 7.440 | 7.274 | 7.274 | 1.228 | 1.036 | 1.762 |
| 20 | 0.1-0.01 | 95.325 | 95.267 | 103.430 | 63.616 | 63.549 | 63.549 |

[a]Isotropic cross section.
[b]Diagonal-transport cross section.
[c]Current-weighted average full-transport cross section.

Figures 11-16 compare the relative errors in the gamma flux with the flux from a $P_1S_4$ solution for energy groups 12 and 17 and the total flux. The flux differences in the core (Figs. 11, 13, and 15), already relatively small, even when isotropic or diagonal-transport-approximation cross sections are used, are further reduced when any one of the full-transport schemes is used. The major benefits of the full-transport method are seen in the reflector region (Figs. 12, 14, and 16), where rather large relative errors are considerably reduced. In group 12, for example, the maximum relative error in the reflector (Fig. 12) is -16.7% for the isotropic ($P_0$) calculation, -12.5% for the diagonal-transport ($P_0^T$) calculation, 1.9% for the full-transport calculation using diagonal-transport currents ($P_0^F$, $P_0^T$), -1.1% for the full-transport calculation using $P_1$ currents ($P_0^F$, $P_1$), and -1.1% for the full-transport calculation using average full-transport cross sections and diagonal-transport currents ($\langle P_0^F \rangle$, $P_0^T$). The reduction in the relative flux errors, expecially in the reflector region, with a full-transport calculation using $P_1$ currents as compared to the reduction in relative flux error with a full-transport calculation using diagonal-transport currents is much smaller than the reduction in relative error when going from a diagonal-transport calculation to a full-transport calculation.

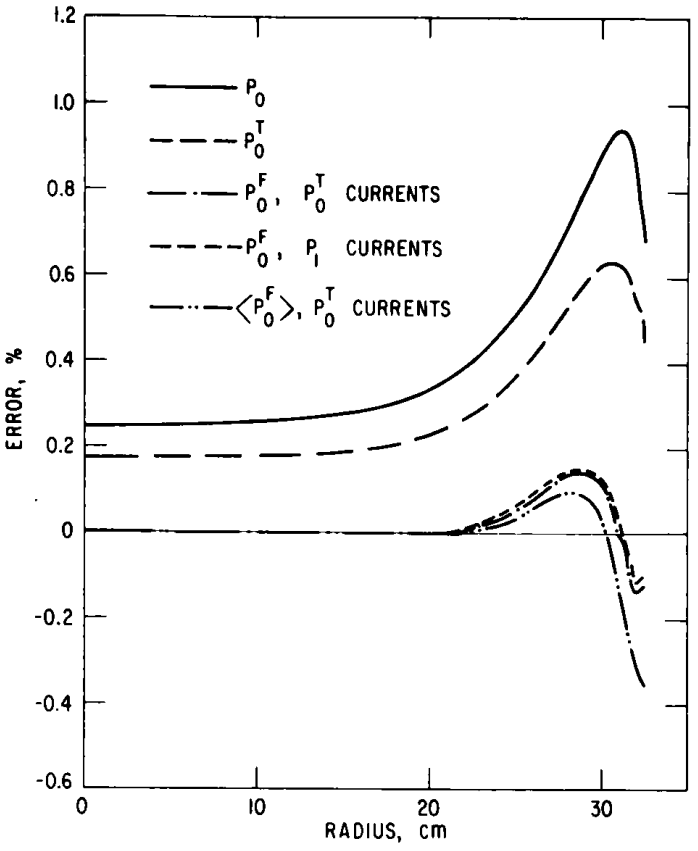


Fig. 11. Errors in Calculated Gamma Flux in Core Relative to Results from $P_1S_4$ Solution: Energy Group 12

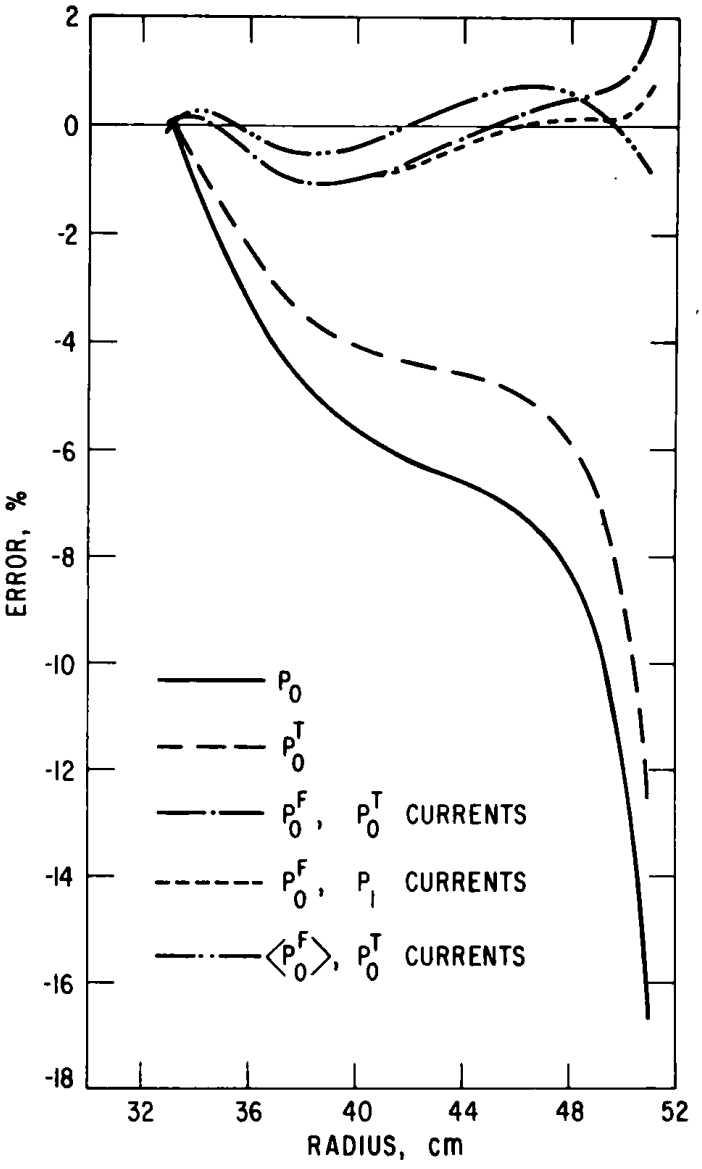


Fig. 12. Errors in Calculated Gamma Flux in Reflector Relative to Results from $P_1S_4$ Solution: Energy Group 12

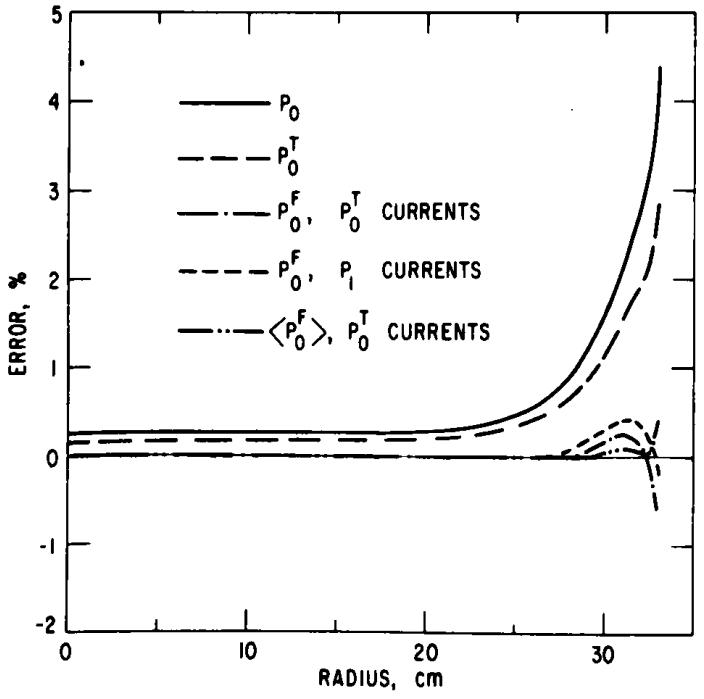


Fig. 13

Errors in Calculated Gamma Flux in Core Relative to Results from $P_1S_4$ Solution: Energy Group 17

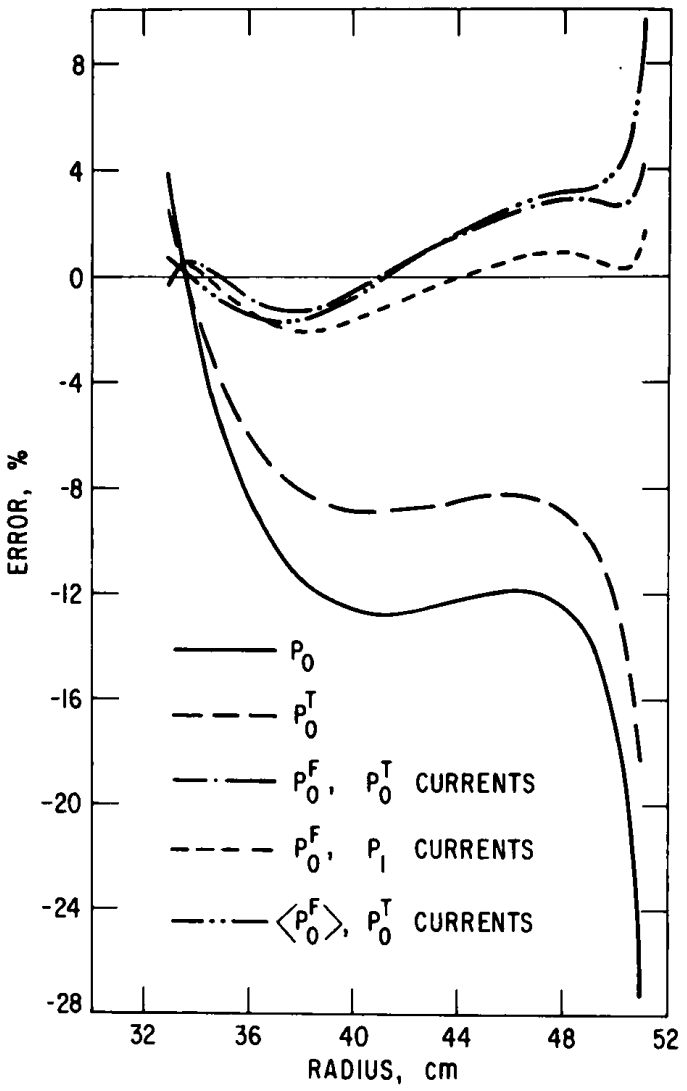


Fig. 14. Errors in Calculated Gamma Flux in Reflector Relative to Results from $P_1S_4$ Solution: Energy Group 17

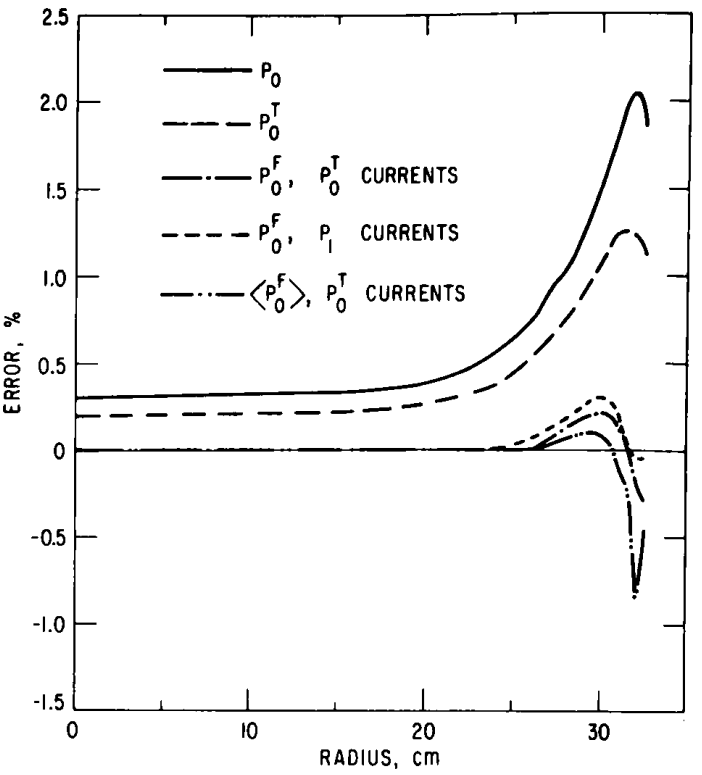


Fig. 15. Errors in Calculated Gamma Flux in Core Relative to Results from $P_1S_4$ Solution: Total Flux

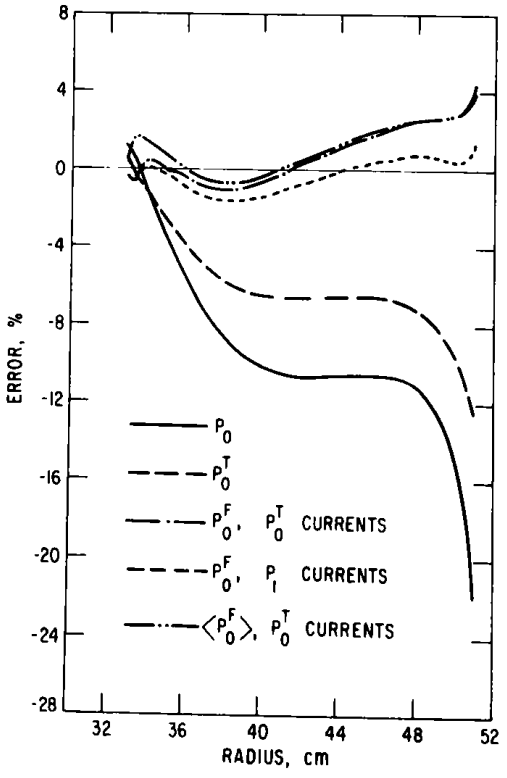


Fig. 16

Errors in Calculated Gamma Flux in Reflector Relative to Results from $P_1S_4$ Solution: Total Flux

Table V compares relative calculation time and cross-section storage requirements to those for a $P_1S_4$ calculation. It is seen that the pointwise full-transport calculations ($P_0^F$) take more time and need more storage than a $P_1S_4$ calculation. The average full-transport calculation ($\langle P_0^F \rangle$) requires about 96% of the calculation time (or essentially the same calculational time) as a $P_1S_4$ calculation, but the cross-section storage requirements are 50% less.

TABLE V. Calculation Times and Cross-section Storage Requirements Relative to Those for a $P_1S_4$ Calculation

| Calculation Type | Averaging Currents | Relative Time | Relative Cross-section Storage Needs |
|---|---|---|---|
| $P_1S_4$ | - | 1.00 | 1.0 |
| $P_0^F$ | $P_1$ | 1.20 | 15.0 |
| $P_0^F$ | $P_0^T$ | 1.24 | 15.0 |
| $\langle P_0^F \rangle$ | $P_0^T$ | 0.96 | 0.5 |
| $P_0^T$ | - | 0.89 | 0.5 |
| $P_0$ | - | 0.92 | 0.5 |

## VI. CONCLUSIONS

Gamma fluxes calculated using the full-transport isotropic cross sections described in this report can be very close to those from a $P_1$ solution. However, care must be taken in using the full-transport-approximation cross sections, because pointwise and regionwise failures may occur. In the model calculation, few modifications were made to the full-transport cross sections, but this may not always be the case. The number of modifications is dependent on the relative magnitudes and shapes of the assumed currents.

The use of full-transport cross sections requires a current, preferably the current that would be obtained upon solution of the problem. However, this limitation is not serious if the calculations are to be done for a system such as EBR-II. The EBR-II reactor changes core loadings frequently, but the relative changes are minor. Hence, the current from a previous loading could be used as the current for the next calculation. The error introduced by using this current estimate would probably be negligible compared to the relative error resulting from the use of diagonal-transport cross sections. If only an isotropic capability is available, an approximate $P_1$ solution can be obtained by running two successive isotropic calculations (a diagonal-transport calculation for the currents and a full-transport calculation for the flux), since the currents obtained from a diagonal-transport solution are sufficiently accurate for evaluating the full-transport cross sections.

The use of the average full-transport cross sections reduces the amount of computer cross-section storage needed to do a calculation. The

maximum relative flux errors are larger than the relative errors obtained when pointwise full-transport cross sections are used, but are still small in comparison to those for a diagonal-transport solution. If a calculation has a large number of mesh points, average full-transport cross sections could be used where they are reasonably constant (such as for regions of nearly isotropic flux), and pointwise full-transport cross sections could be used where there is a strong spatial dependence (such as for regions of highly anisotropic flux).

## REFERENCES


1. D. Meneghetti and W. B. Loewenstein, "EBR-II Physics Experience," *Proc. Int. Symp. Physics of Fast Reactors*, Tokyo, Oct 16-19, 1973, Vol. 1, p. 175 (1973).
2. W. W. Engle, *ANISN, A One-dimensional Discrete Ordinates Transport Code with Anisotropic Scattering*, K-1693, Oak Ridge National Laboratory (Mar 1967).
3. W. E. Ford III, *The POPOP4 Library of Neutron Induced Secondary Gamma-ray Yield and Cross Section Data*, CTC-42, Oak Ridge National Laboratory (Sept 1970).
4. W. E. Ford III and D. H. Wallace, *POPOP4, A Code for Converting Gamma-ray Spectra to Secondary Gamma-ray Production Cross Sections*, CTC-12, Oak Ridge National Laboratory (May 1969).
5. B. J. Toppel, A. L. Rago, and D. M. O'Shea, *$MC^2$, A Code to Calculate Multigroup Cross Sections*, ANL-7318 (June 1967).
6. J. R. Knight and F. R. Mynatt, *MUG, A Program for Generating Multigroup Photon Cross Sections*, CTC-17, Oak Ridge National Laboratory (Jan 1970).
7. R. V. Meghreblian and D. K. Holmes, *Transport Theory*, Chapter 7: Reactor Analysis, McGraw-Hill, New York (1960).

## Distribution of ANL-77-88

Internal:

J. A. Kyger
R. Avery
L. Burris
S. A. Davis
B. R. T. Frost
D. C. Rardin
R. J. Teunis
C. E. Till
R. S. Zeno
C. E. Dickerman
H. K. Fauske
S. Fistedis
B. D. LaMar
J. F. Marchaterre
H. O. Monson
R. Sevy
B. J. Toppel
A. E. Allen
W. N. Beck
D. B. Berg
P. R. Betten
W. F. Booty
J. H. Bottcher
F. L. Brown
L. K. Chang
D. W. Cissel
D. C. Cutforth
E. M. Dean
A. L. Doster
J. W. Driscoll (3)
E. E. Feldman
A. J. Foltman
F. C. Franklin
R. M. Fryer
J. L. Gillette
G. H. Golden
K. N. Grimm (5)
K. C. Gross
G. L. Hofman
E. Hutter
F. S. Kirn
J. H. Kittel
J. F. Koenig
J. A. Koerner
D. A. Kucera
E. W. Laird
J. D. B. Lambert
H. A. Larson
W. K. Lehto
D. Meneghetti (5)
F. Metcalf
D. Mohr
K. J. Moriarty
K. E. Phillips
C. C. Price
R. H. Rempert
R. E. Rice
W. E. Ruther
J. I. Sackett
W. R. Simmons
R. M. Singer
R. N. Smith
R. R. Smith
B. Y. C. So
R. V. Strain
J. E. Sullivan
J. V. Tokar
G. W. Trimble
R. J. McConnell
T-S. Wu
A. B. Krisciunas
ANL Contract File
ANL Libraries (5)
TIS Files (6)

External:

DOE-TIC, for distribution per UC-79d (264)
Manager, Chicago Operations Office
Chief, Chicago Patent Group
Director, Reactor Programs Div., CH
Director, CH-INEL
Director, DOE-RRT (2)
President, Argonne Universities Association
EBR-II Project Review Committee:
- E. L. Alexanderson, Detroit Edison Co.
- J. R. Calhoun, Tennessee Valley Authority
- D. T. Eggen, Northwestern U.
- W. H. Jens, Detroit Edison Co.
- L. J. Koch, Illinois Power Co.
- H. Pearlman, Atomics International
- F. J. Remick, Pennsylvania State U.